ChemComm

COMMUNICATION

View Article Online
View Journal | View Issue

Cite this: *Chem. Commun.*, 2018, **54**, 479

Received 10th November 2017,
Accepted 10th December 2017

DOI: 10.1039/c7cc08675j

rsc.li/chemcomm

Ca–Al double-substituted strontium hexaferrites with giant coercivity†

Lev A. Trusov, *[a] Evgeny A. Gorbachev,[b] Vasily A. Lebedev,[a] Anastasia E. Sleptsova,[b] Ilya V. Roslyakov,[a] Ekaterina S. Kozlyakova,[c] Alexander V. Vasiliev,[a] Robert E. Dinnebier,[d] Martin Jansen[d] and Pavel E. Kazin[a]

We demonstrate that the simultaneous substitution of calcium and aluminum for strontium and iron in strontium hexaferrite results in a significant increase of coercivity up to a record high of 21.3 kOe. We propose that the effect is originated from a crystal structure distortion causing an increase of the magnetocrystalline anisotropy.

Magnetic materials with large coercivity have broad applications ranging from permanent magnets and data storage media to high-frequency electromagnetic wave filters. The most widely used hard magnetic materials are metallic and contain rare-earth elements (*e.g.* $Nd_2Fe_{14}B$ or $SmCo_5$ and Sm_2Co_{17}) or noble metals (*e.g.* FePt or CoPt).[1] Such materials exhibit a large magnetocrystalline anisotropy, high magnetization and coercivity. However, the high costs and shortage of some of the constitutive metals impel to search for new materials or to improve the known materials that do not contain these elements. Low-cost M-type hexaferrites are widely used for magnet production; however, their magnetization and coercivity are much lower than those of the materials mentioned above, limiting hexaferrites to special applications.

The only known ferrite material exhibiting coercivity higher than 20 kOe (also considered as "giant coercive force") at room temperatures is ε-Fe_2O_3.[2,3] The large coercivity is the result of high magnetocrystalline anisotropy ($K_1 \approx 2$–7.7×10^6 erg cm^{-3}) and relatively low saturation magnetization ($M_S \approx 15$ emu g^{-1}), since coercive force H_C is proportional to K_1/M_S.[1] However, the production of ε-Fe_2O_3 is quite complex, generally involving particle formation in a mesoporous amorphous silica matrix and subsequent removal of silica.[3]

M-Type hexaferrites ($MFe_{12}O_{19}$, M = Ba, Sr, and Pb) exhibit a high magnetocrystalline anisotropy ($K_1 \approx 3.6 \times 10^6$ erg cm^{-3}) but their coercivity is significantly lower due to their higher magnetization ($M_S \approx 70$ emu g^{-1}), and rarely exceeds 6 kOe.[4,5] It is known that a controllable decrease of the magnetization *via* partial substitution of iron atoms with aluminum may lead to a significant increase of the coercivity.[6,7] However, due to low reactivity, high temperatures are required for incorporating aluminum into the hexaferrite. This leads to fast crystallite growth, and the crystallite size exceeds the single-domain limit abruptly lowering the coercive force. Furthermore, there is an issue of unreacted impurities at high aluminum content, which additionally decrease the material magnetization. Recently it was shown that the coercivities of aluminum-substituted hexaferrites approaches 18.1 kOe at a saturation magnetization of 9 emu g^{-1};[7] however, these values fall below the typical characteristics of ε-Fe_2O_3. Here we report an efficient synthesis of Al and Ca–Al substituted strontium hexaferrites, the coercivities of which increase up to 21.3 kOe. We further describe the features of the microstructure and crystal structure of the materials and discuss their influence on the magnetic properties.

The samples were prepared using the citrate melt auto-ignition method. Aqueous solutions of Ca, Sr, Fe and Al nitrates (Sigma-Aldrich) were mixed with citric acid (Sigma-Aldrich) to give a molar ratio of metal ions to citrate ions of 1 : 3. Then ammonia solution was added until the pH 7. Subsequently the solutions were heated in a sand bath to evaporate water. The viscous citrate melts formed ignited turning into lightweight black powders. The precursor mixtures were heated to 1200 °C with a rate of 20 °C min^{-1} and annealed for 24 hours. The compositions of the as-prepared samples were $SrFe_{12-x}Al_xO_{19}$ (Series 1) and $Sr_{1-x/12}Ca_{x/12}Fe_{12-x}Al_xO_{19}$ (Series 2), where x = 1.5, 2, 3, 3.5 and 4. The Ca containing Series 2 is designed to keep the equal mole fraction of the substituted Sr and Fe ions. According to X-ray powder diffraction phase analysis, the samples represent M-type hexaferrite phases (ICDD card 84-1531) with negligible content of impurities in some samples. The crystal lattice parameters decrease nearly linearly with the aluminum and calcium substitution (Fig. S1, ESI†), as the Al^{3+} ion radius (r^{VI} = 0.535 Å) is smaller than that of Fe^{3+} (r^{VI} = 0.645 Å) and the

[a] *Faculty of Chemistry, Moscow State University, Moscow, 119991, Russia. E-mail: trusov@inorg.chem.msu.ru*
[b] *Faculty of Materials Science, Moscow State University, Moscow, 119991, Russia*
[c] *Faculty of Physics, Moscow State University, Moscow, 119991, Russia*
[d] *Max Planck Institute for Solid State Research, Stuttgart, 70569, Germany*

† Electronic supplementary information (ESI) available: Experimental details, Table S1 and Fig. S1–S4. See DOI: 10.1039/c7cc08675j

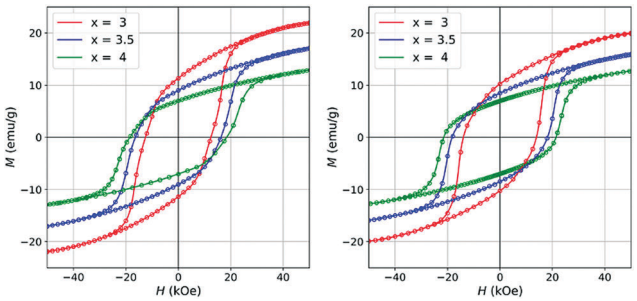

Fig. 1 $M(H)$ curves of the samples: $SrFe_{12-x}Al_xO_{19}$ (left) and $Sr_{1-x/12}Ca_{x/12}Fe_{12-x}Al_xO_{19}$ (right) (Series 1 and 2, correspondingly).

Ca^{2+} ion (r^{XII} = 1.34 Å) is smaller than Sr^{2+} (r^{XII} = 1.44 Å).[8] This indicates the presence of continuous solid solutions for both sample series, at least for $x < 4$.

The magnetic hysteresis curves of the samples are shown in Fig. 1 and the corresponding data are summarized in Table 1. The shapes of hysteresis loops are typical for randomly oriented single-domain Stoner–Wohlfarth particles with $M_r/M_s \approx 0.5$.[1] The saturation magnetization drops with growing aluminum content, while the coercivity increases and reaches 18.5 kOe for the $SrFe_8Al_4O_{19}$ sample. The introduction of Ca leads to a further coercivity increase of up to 21.3 kOe for $Sr_{0.67}Ca_{0.33}Fe_8Al_4O_{19}$. It is noteworthy that the saturation magnetization (M_S = 14 emu g^{-1} at 70 kOe) at x = 4 is significantly higher than that reported earlier for the same level of Al substitution in hexaferrites.[7] The values of M_s and H_c for the $Sr_{0.67}Ca_{0.33}Fe_8Al_4O_{19}$ sample are nearly the same as those reported for the pure ε-Fe_2O_3 phase (M_s = 15 emu g^{-1} at 70 kOe, H_c = 20 kOe).[2,3] The only ferrite material revealing a higher coercive force at room temperature (up to 27 kOe) is Rh-substituted ε-Fe_2O_3; however, its saturation magnetization is considerably lower (7 emu g^{-1}).[9]

Let us discuss the factors that influence the formation of the hexaferrites with giant coercivity. First of all, the synthesis conditions are crucial for obtaining single-domain hexaferrite particles (with diameters below critical $d_{cr} \approx 500$ nm for pure hexaferrite[4,7]). We used a relatively high amount of citric acid during the preparation of the precursors, which allowed us to obtain highly porous carbon-rich intermediate products (Fig. 2a). The porous morphology obviously survived the high temperature treatment, ensuring a low degree of particle agglomeration (Fig. 2b and c). The bulk density of the as-prepared powders is about 5% of the crystallographic values. The high initial porosity of the precursors led to suppression of diffusion inside the walls of the pores and resulted in a formation of fine particles, in spite of the temperature as high as 1200 °C was applied.[4,5] On the other hand, the high temperature is highly favourable for the formation of single-phase hexaferrite particles, which are free of structural defects lowering coercivity. The heating mode also matters, thus, in contrast to smooth heating, placing the precursor straight into the hot furnace leads to a breakdown of its porous structure and results in highly sintered materials (Fig. 2d) with large particle diameters (>2000 nm) and, consequently, low coercivity.

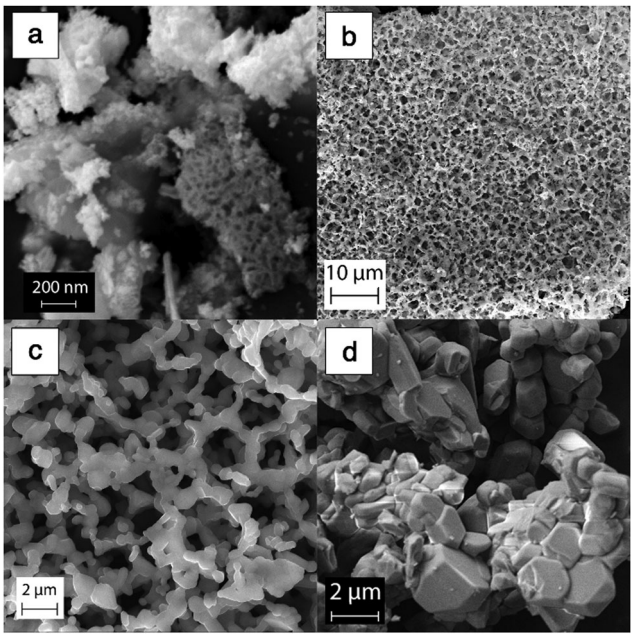

Fig. 2 Typical SEM images: (a) intermediate product, (b and c) as-prepared hexaferrite annealed at heating mode, and (d) hexaferrite annealed isothermally at 1200 °C (sample $Sr_{0.67}Ca_{0.33}Fe_8Al_4O_{19}$).

Table 1 Magnetic properties and mean particle diameter of hexaferrite samples

Series[a]	x	M_S[b] (emu g^{-1})	M_R (emu g^{-1})	H_C (kOe)	d[c] (nm)
1	1.5	47.5	23.9	9.1	590
	2	38.5	19.4	9.8	620
	3	21.9	11.3	12.5	400
	3.5	17.0	9.0	16.3	370
	4	12.9	7.0	18.5	480
2	1.5	47.3	23.7	9.3	620
	2	37.8	19.1	10.2	640
	3	19.9	10.2	13.6	630
	3.5	15.9	8.5	18.0	720
	4	12.7	7.0	21.3	680

[a] $SrFe_{12-x}Al_xO_{19}$ (Series 1) and $Sr_{1-x/12}Ca_{x/12}Fe_{12-x}Al_xO_{19}$ (Series 2). [b] Magnetization at 50 kOe. [c] See typical distributions in Fig. S2, ESI.

The samples containing Ca (Series 2) definitely display a higher coercivity, and for x = 4 the increase amounts to 15%. This may be connected both with morphological as well as crystal structure features. The shape analysis of the magnetic hysteresis loops by plotting magnetic susceptibility $\chi = dM/dH$ *versus* H allows the extraction of the switching field distribution, which reflects particle coercivity distribution in the samples (Fig. 3). As can be seen, the samples without calcium (Series 1) show broader coercivity distributions with an extended low-coercivity side, and it is observed for each aluminum content. A potential reason may be a broader size distribution and the presence of low-coercivity particles with sizes exceeding the single-domain limit. However, according to scanning electron microscopy, the samples with calcium (Series 2) contain noticeably larger particles (Table 1 and Fig. S2, ESI†), while their coercivity is higher and more uniform. Moreover, the single-domain limit d_{cr}

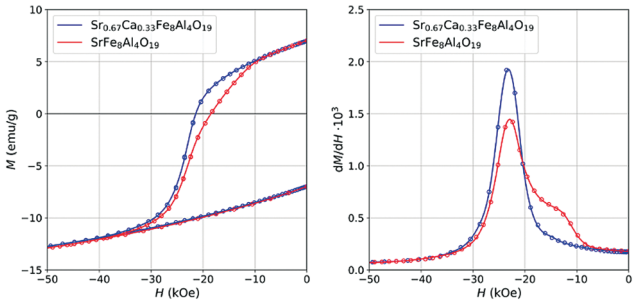

Fig. 3 $M(H)$ (left) and dM/dH (right) *vs.* H curves of $SrFe_8Al_4O_{19}$ (red line) and $Sr_{0.67}Ca_{0.33}Fe_8Al_4O_{19}$ (blue line).

should grow along with the aluminum content.[10] Thus, it appears unlikely that the wider coercivity distribution of the samples without calcium is caused by the size distribution. An explanation could rather be connected to the inhomogeneity of the aluminum distribution, which should also cause a wider coercivity distribution. The chemical inhomogeneity of the doped hexaferrite samples can be traced back to details of the temperature schedule during synthesis, which basically consists of two steps, the heating up and the high-temperature annealing. The solid state reaction of hexaferrite formation starts at temperatures of about 800 °C,[11] and at this stage the resulting phase is expected to contain a low amount of aluminum.[12] At higher temperatures the formation of highly substituted hexaferrite occurs and during the subsequent 24 h annealing the homogenization of the composition takes place. It is known that calcium improves the reactivity and sintering of hexaferrite ceramics,[13,14] so we can expect a better compositional homogeneity of the Ca-containing samples. To confirm the role of calcium, we synthesized the sample $Sr_{0.67}Ca_{0.33}Fe_8Al_4O_{19}$ at 1100 °C, when the diffusion is slower compared to that at 1200 °C. The resulting hysteresis loop and coercivity distribution are shown in Fig. 4. The coercivity distribution of the sample annealed at 1100 °C is much wider than that of the sample annealed at 1200 °C, while the apparent coercivity is very close and these values are much higher than the coercivity of $SrFe_8Al_4O_{19}$. So the broad coercivity distribution in Al-substituted hexaferrites is most likely due to the solid solution inhomogeneity, and the higher coercivity of Ca–Al substituted hexaferrites is not caused by the particle morphology. Thus, the effect of the coercivity

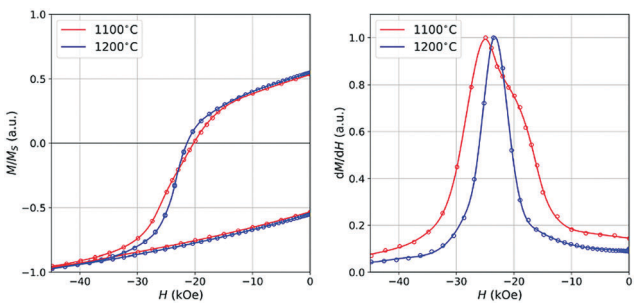

Fig. 4 $M(H)$ (left) and dM/dH (right) *vs.* H curves of the $Sr_{0.67}Ca_{0.33}Fe_8Al_4O_{19}$ sample annealed at 1100 °C (red line) and at 1200 °C (blue line).

increase is most probably connected to an enhancement of the magnetocrystalline anisotropy constant caused by calcium introduction into the hexaferrite structure.

The crystal structure parameters of the high-coercivity samples were refined *via* the Rietveld method using high-precision powder diffraction data and the Jana2006 software[15] (Fig. S3, ESI†). In the hexaferrite structure, iron ions occupy five non-equivalent sites: three of them are octahedral (12k, 2a and $4f_2$), one is tetrahedral ($4f_1$) and one is trigonal bipyramidal (2b).[16] Hexaferrites are ferrimagnetic, so the 12k, 2a and 2b sites have the upward electron spin direction while the $4f_1$ and $4f_2$ ones have downward spins. The introduction of diamagnetic Al^{3+} ions modifies the net magnetization of the material. In addition, the presence of aluminum reduces superexchange interactions within iron sublattices, which leads to a decrease of magnetization and a decrease of T_c.[7] We found that the Curie temperature indeed linearly decreases with the aluminum content in both composition series (Fig. S4, ESI†) and it extrapolates to zero at $x = 12$. The results of crystal structure refinement are summarized in Table S1, ESI† and Table 2. For Al-substituted samples (Series 1) the distributions are close to those reported previously:[6,17] aluminum enters preferably into the octahedral 2a and 12k sites. Since Fe ions in these sites have uncompensated upward spins, the substitution leads to a corresponding reduction of magnetization.

The substitution in our samples shows higher site selectivity than that reported earlier for ceramic samples,[17] most likely due to the lower synthesis temperature. And we have not found any significant difference in aluminum distribution between the Al (Series 1) and Ca–Al (Series 2) substituted samples.

Considering a single-ion model of magnetocrystalline anisotropy of hexaferrite, it was found that the iron ion in the bipyramidal 2b site (Fe2) plays a decisive role.[18,19] Strictly speaking, cations at the bipyramidal site are not placed directly in the center, but are distributed between the two adjacent pseudotetrahedra (so-called 4e sites).[16] In any case, in this site, the crystal field has a pronounced axial component and provides negative zero field splitting of a few cm^{-1} determining an easy magnetization direction along the c-axis. The splitting is expected to grow with increasing crystal field strength exerted by both the equatorial and apical oxygen atoms. It is known that the replacement of barium in $BaFe_{12}O_{19}$ by strontium results in an increase of the magnetocrystalline constant K_1 from 3.25×10^6 erg cm^{-3} to 3.57×10^6 erg cm^{-3}, which is in accordance with strontium hexaferrite materials usually exhibiting a higher coercivity. This may be due to the smaller radius of the strontium ion, which results in lattice contraction and a decrease in the separation between the iron and equatorial oxygen atoms (Fe2–O3) in the 2b bipyramidal site.[16] This induces an enlargement of the crystal field strength and thus of the magnetic anisotropy. Similarly, in Al-substituted hexaferrites the substitution of calcium for strontium leads to an analogous effect of the Fe2–O3 distance shortening (Table 2 and Fig. 5). So, the Ca–Al double substituted hexaferrites should have higher K_1 values at the same Al content. And the higher coercivity of Ca–Al substituted compounds can be explained by the larger magnetocrystalline anisotropy.‡

Table 2 Lattice parameters and selected bond lengths

Series[a]	x	a, Å	c, Å	α-Fe_2O_3, wt%	M2–M2,[b] Å	O1–O1, Å	M2–O3,[b] Å
1	3	5.8121(2)	22.8075(8)	0	0.356(11)	4.576(14)	1.840(10)
	3.5	5.8000(1)	22.7657(3)	<1	0.383(11)	4.581(11)	1.834(9)
	4	5.7882(1)	22.7298(4)	0	0.407(11)	4.591(12)	1.835(10)
2	3	5.8099(1)	22.7843(7)	1.9	0.342(10)	4.568(13)	1.839(12)
	3.5	5.7966(1)	22,7410(4)	3.3	0.381(15)	4.587(16)	1.831(13)
	4	5.7858(1)	22.7016(3)	<1	0.387(9)	4.541(10)	1.816(8)
$BaFe_{12}O_{19}$[c]					0.340(1)	4.596(3)	1.867(2)
$SrFe_{12}O_{19}$[c]					0.194(10)	4.536(7)	1.854(1)
$SrAl_{12}O_{19}$[d]					0.424(4)	4.475(4)	1.765(3)
$CaAl_{12}O_{19}$[e]					0.338(2)	4.419(2)	1.751(1)

[a] $SrFe_{12-x}Al_xO_{19}$ (Series 1) and $Sr_{1-x/12}Ca_{x/12}Fe_{12-x}Al_xO_{19}$ (Series 2). [b] M = Fe^{3+} or Al^{3+}. [c] From ref. 16. [d] From ref. 20. [e] From ref. 21.

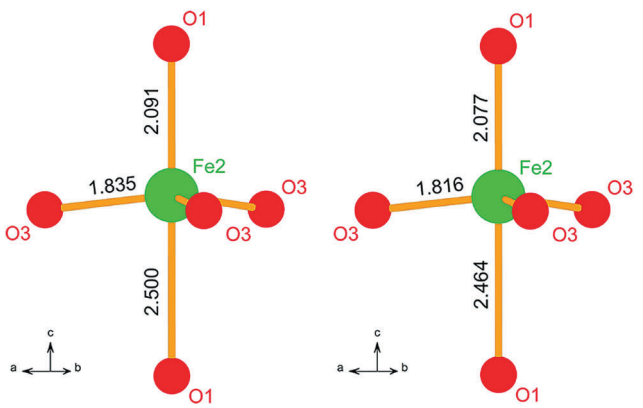

Fig. 5 Representation of bipyramidal site 2b (Fe2) in $SrFe_8Al_4O_{19}$ (left) and $Sr_{0.67}Ca_{0.33}Fe_8Al_4O_{19}$ (right).

In summary, we have obtained Ca–Al substituted strontium hexaferrites, the coercivities of which reach the giant value of 21.3 kOe at the saturation magnetization of 14 emu g^{-1}. We have shown that the presence of Ca ions leads to shrinking of the iron surrounding the 2b site, which causes a higher magnetocrystalline anisotropy and thus enhances the coercive force. Apart from the fact that the phenomenon attracts pure scientific interest, the obtained material possesses one of the highest values of coercivity among the hard-magnetic ferrites and it is fully compatible with the common ferrite technology; therefore, since the optimized materials presented here exclusively comprise abundant elements, it may at least be of interest for some special purpose applications, *e.g.* high-frequency electromagnetic wave absorbers or highly stable magnetic recording.

Conflicts of interest

There are no conflicts to declare.

Notes and references

‡ Further details of the crystal structure investigations may be obtained from the Fachinformationszentrum Karlsruhe, 76344 Eggenstein-Leopoldshafen, Germany (Fax: +49-7247-808-666; E-Mail: crysdata@fizkarlsruhe.de, http://www.fizkarlsruhe.de/request for deposited data.html) on quoting the depository number CSD 433755–433760.

1 K. H. J. Buschow and F. R. de Boer, *Physics of Magnetism and Magnetic Materials*, Kluwer Academic/Plenum Publishers, New York, 2003.
2 J. Jin, S. Ohkoshi and K. Hashimoto, *Adv. Mater.*, 2004, **16**, 48.
3 J. Tuček, R. Zbořil, A. Namai and S. Ohkoshi, *Chem. Mater.*, 2010, **22**, 6483.
4 T. Koutzarova, S. Kolev, C. Ghelev, K. Grigorov and I. Nedkov, in *Advances in Nanoscale Magnetism*, ed. B. Aktas and F. Mikailov, Springer, Berlin Heidelberg, 2009, p. 183.
5 R. C. Pullar, *Prog. Mater. Sci.*, 2012, **57**, 1191.
6 P. E. Kazin, L. A. Trusov, D. D. Zaitsev, Y. D. Tretyakov and M. Jansen, *J. Magn. Magn. Mater.*, 2008, **320**, 1068.
7 H. Luo, B. K. Rai, S. R. Mishra, V. V. Nguyen and J. P. Liu, *J. Magn. Magn. Mater.*, 2012, **324**, 2602.
8 R. D. Shannon, *Acta Crystallogr., Sect. A: Cryst. Phys., Diffr., Theor. Gen. Crystallogr.*, 1976, **32**, 751.
9 A. Namai, M. Yoshikiyo, K. Yamada, S. Sakurai, T. Goto, T. Yoshida, T. Miyazaki, M. Nakajima., T. Suemoto, H. Tokoro and S. Ohkoshi, *Nat. Commun.*, 2012, **3**, 1035.
10 J. N. Dahal, L. Wang, S. R. Mishra, V. V. Nguyen and J. P. Liu, *J. Alloys Compd.*, 2014, **595**, 213.
11 H. Kojima, in *Ferromagnetic Materials*, ed. E. P. Wohlfarth, North-Holland Publishing Company, Amsterdam, 1982, vol. 3.
12 H. Z. Wang, B. Yao, Y. Xu, Q. He, G. H. Wen, S. W. Long, J. Fan, G. D. Li, L. Shan, B. Liu, L. N. Jiang and L. L. Gao, *J. Alloys Compd.*, 2012, **537**, 43.
13 G. Asti, M. Carbucchio, A. Deriu, E. Lucchini and G. Slokar, *J. Magn. Magn. Mater.*, 1980, **20**, 44.
14 J. Töpfer, S. Schwarzer, S. Senz. and D. Hesse, *J. Eur. Ceram. Soc.*, 2005, **25**, 1681.
15 V. Petricek, M. Dusek and L. Palatinus, *Z. Kristallogr.*, 2014, **229**, 345.
16 X. Obradors, X. Solans, A. Collomb, D. Samaras, J. Rodriguez, M. Pernet and M. Font-Altaba, *J. Solid State Chem.*, 1988, **72**, 218.
17 F. Sandiumenge, S. Gali and J. Rodriguez, *Mater. Res. Bull.*, 1988, **23**, 685.
18 N. Fuchikami, *J. Phys. Soc. Jpn.*, 1965, **20**, 760.
19 Y. Xu, G. Yang, D. Chu and H. Zhai, *Phys. Status Solidi B*, 1990, **157**, 685.
20 K. Kimura, M. Ohgaki, K. Tanaka, H. Morikawa and F. Marumo, *J. Solid State Chem.*, 1990, **87**, 186.
21 A. Utsunomiya, K. Tanaka, H. Morikawa, F. Marumo and H. Kojima, *J. Solid State Chem.*, 1988, **75**, 197.